Fer1l6 is essential for the development of vertebrate muscle tissue in zebrafish

Josephine A. Bonventre[a], Chelsea Holman[a], Aayushi Manchanda[b], Sara J. Codding[a], Trisha Chau[a], Jacob Huegel[a], Carrie Barton[c], Robert Tanguay[c], and Colin P. Johnson[a,b,*]

[a]Department of Biochemistry and Biophysics, [b]Molecular and Cellular Biology Program, and [c]Department of Environmental and Molecular Toxicology, Oregon State University, Corvallis, OR 97331

ABSTRACT **The precise spatial and temporal expression of genes is essential for proper organismal development. Despite their importance, however, many developmental genes have yet to be identified. We have determined that Fer1l6, a member of the ferlin family of genes, is a novel factor in zebrafish development. We find that Fer1l6 is expressed broadly in the trunk and head of zebrafish larvae and is more restricted to gills and female gonads in adult zebrafish. Using both genetic mutant and morpholino knockdown models, we found that loss of Fer1l6 led to deformation of striated muscle tissues, delayed development of the heart, and high morbidity. Further, expression of genes associated with muscle cell proliferation and differentiation were affected. Fer1l6 was also detected in the C2C12 cell line, and unlike other ferlin homologues, we found Fer1l6 expression was independent of the myoblast-to-myotube transition. Finally, analysis of cell and recombinant protein–based assays indicate that Fer1l6 colocalizes with syntaxin 4 and vinculin, and that the putative C2 domains interact with lipid membranes. We conclude that Fer1l6 has diverged from other vertebrate ferlins to play an essential role in zebrafish skeletal and cardiac muscle development.**

Monitoring Editor
Marianne Bronner
California Institute of Technology

Received: Jun 28, 2018
Revised: Oct 30, 2018
Accepted: Nov 29, 2018

INTRODUCTION

Gene duplication is a common event in molecular biology, with subsequent functional diversification allowing for the adoption of new abilities. This process is epitomized in the ferlin gene family. Ferlins are eukaryotic membrane trafficking proteins composed of three to seven calcium binding C2 domains (Lek *et al.*, 2012; Johnson, 2017). First identified as a fertility factor in *Caenorhabditis elegans* and *Drosophila melanogaster*, gene duplication events have expanded the family to include six members in mammals (dysferlin, otoferlin, myoferlin, Fer1l4, Fer1l5, and Fer1l6) with divergent tissue expression patterns and function (Washington and Ward, 2006; Smith and Wakimoto, 2007; Lek *et al.*, 2010). Within this family, otoferlin, myoferlin, and dysferlin have been the focus of intense study due to their link to human pathologies. Otoferlin is expressed almost exclusively in sensory hair cells, where it regulates calcium sensitive synaptic vesicle fusion during the process of hearing (Roux *et al.*, 2006; Chatterjee *et al.*, 2015; Hams *et al.*, 2017). Dozens of mutations in the otoferlin gene have been linked to congenital nonsyndromic hearing loss (Yasunaga *et al.*, 1999; Rodríguez-Ballesteros *et al.*, 2008; Marlin *et al.*, 2010). By contrast, dysferlin is expressed most prominently in muscle tissue, where its C2 domains are thought to function in the repair of damaged sarcolemma and in modulating calcium channel activity (Bansal and Campbell, 2004; Kerr *et al.*, 2013). Numerous mutations in dysferlin have been directly linked to muscle-related diseases including limb-girdle muscular dystrophy, Miyashi myopathy, distal anterior compartment myopathy, and dilated cardiomyopathy (Anderson *et al.*, 1999; Bansal and Campbell, 2004; Cacciottolo *et al.*, 2011). Myoferlin is more widely expressed than otoferlin or dysferlin and functions in endosome dynamics, tyrosine kinase recycling, and myotube formation (Davis *et al.*, 2000; Doherty *et al.*, 2005; Yu *et al.*, 2011). Abnormal expression of myoferlin is correlated with breast cancer and pancreatic adenocarcinoma invasiveness (Turtoi *et al.*, 2013; Wang *et al.*, 2013). Fer1l5 also contributes to endosome recycling and myotube formation (Posey *et al.*, 2011, 2014). Currently, Fer1l4 is designated a

This article was published online ahead of print in MBoC in Press (http://www.molbiolcell.org/cgi/doi/10.1091/mbc.E18-06-0401) on December 5, 2018.

The authors declare no competing interests.

J.A.B., C.P.J., and C.H. designed the experiments. J.A.B., C.H., T.C., S.J.C., and J.H. performed experiments and analyzed the data. J.A.B., C.P.J., and C.H. wrote the manuscript.

*Address correspondence to: Colin P. Johnson (colin.johnson@oregonstate.edu).

Abbreviations used: DAPI, 4′6′-diamidino-2-phenylindole; LB, lysogeny broth; NGS, normal goat serum; PVDF, polyvinylidene fluoride.

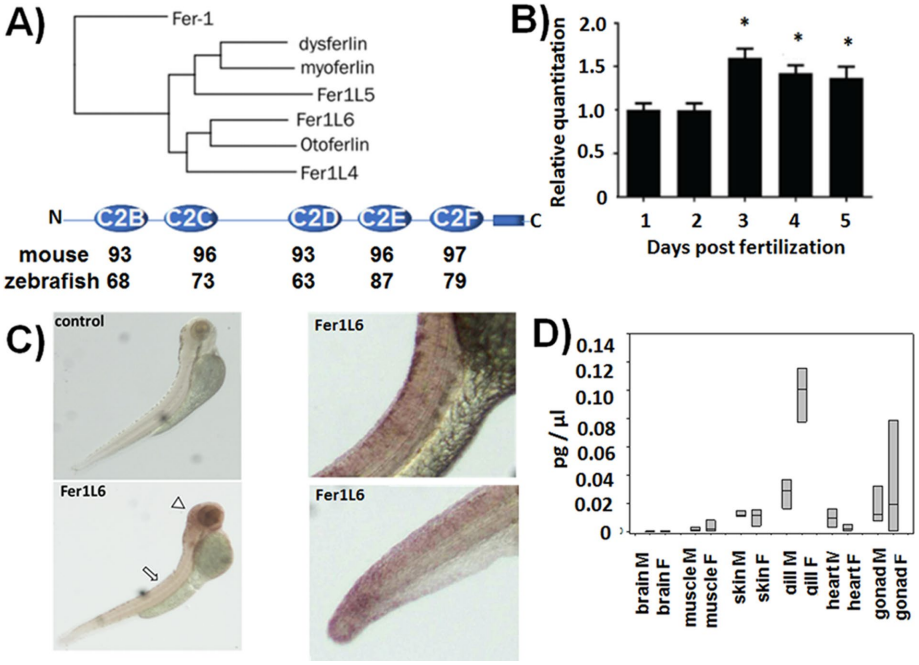

FIGURE 1: Fer1l6 expression in zebrafish. (A) Top, phylogenetic tree of human ferlin proteins and *C. elegans* Fer1 gene. Ensemble transcript IDs were Q17388 for Fer1, ENST00000258104.7 for dysferlin, ENST00000359263.8 for myoferlin, ENST00000624922.3 for Fer1l5, ENST00000522917.5 for Fer1l6, ENST00000272371.6 for otoferlin, and ENST00000615531.4 for Fer1l4. Bottom, schematic of predicted structure for Fer1l6 based on primary sequence. Ovals indicate C2 domains; rectangle indicates transmembrane domain. Percent sequence identity between the predicted C2 domains of human Fer1l6 compared with mouse and zebrafish are shown. (B) Expression of *fer1l6* from whole embryo zebrafish for days 1–5 postfertilization. *, $p < 0.05$ compared with 1 dpf, $n = 3$. (C) In situ hybridization images of zebrafish larvae at 1 dpf. Top left panel is representative of negative control; bottom left panel is a representative image of *fer1l6* stained larvae. Arrow denotes trunk; arrowhead denotes head. Right panels show higher magnification images of the trunk and tail region at 1 dpf. (D) Expression of fer1l6 in adult zebrafish organs quantified using a standard curve ($n = 4$ female, 4 male).

pseudogene and functions as a long-noncoding RNA with a clinical relevance to gastric cancer outcomes, and Fer1l6 remains uncharacterized, preventing a complete picture of the roles ferlins play in vertebrate physiology (Liu *et al.*, 2014; Xia *et al.*, 2015).

The zebrafish (*Danio rerio*) genome includes five distinct ferlin members (dysferlin, otoferlin, myoferlin, Fer1l4, and Fer1l6). The genetic tractability of zebrafish and ease of phenotypic analysis has made zebrafish a valuable organism for the study of uncharacterized vertebrate genes. Here we use a variety of approaches, including genetic mutation, morpholino knockdown, electron microscopy, expression profiling, and recombinant biochemistry to characterize Fer1l6 in zebrafish. We find that Fer1l6 expression is dynamic, with an essential role in early muscle development, and prominent expression in gonads of adult organisms. We conclude that Fer1l6 is a calcium binding membrane trafficking protein that plays an essential function in muscle formation during zebrafish development and is nonredundant with other zebrafish ferlins. Our study also establishes an in vivo model for the study of Fer1l6.

RESULTS AND DISCUSSION

Expression of Fer1l6 in zebrafish

The structure of Fer1l6 is shown in Figure 1A. Amino acid sequence analysis of Fer1l6 indicates conservation between zebrafish and human proteins, with 59% overall sequence identity, and 63–87% sequence identity between predicted C2 domains, suggesting a conserved function in vertebrates (Figure 1A). To determine the relative expression of *fer1l6* throughout development, we conducted reverse transcription quantitative real time-PCR (qRT-PCR) on whole zebrafish larvae. Transcriptional expression of *fer1l6* was detected throughout the 5-d developmental period, with the peak expression occurring on day 3 or ~72 h postfertilization (hpf; Figure 1B). Expression was detected as early as 6 hpf and increased steadily until 24 hpf/1 d postfertilization (dpf; Supplemental Figure 2A). Whole mount in situ hybridization (ISH) for *fer1l6* at 1 dpf revealed a broad spatial expression profile throughout the organism, with the most prominent staining occurring in the head and trunk region (Figure 1, C and D). Adult zebrafish ~1 yr in age were necropsied, and the expression of fer1l6 transcripts in different organs was measured for brain, heart, gill, liver, muscle, skin, stomach/small intestine, and gonad tissue of males and females. *Fer1l6* was detected in all organs tested; however, the greatest expression was observed in gill and gonads (Figure 1E). The gill showed a significant sex-specific difference in *fer1l6* expression, and female gonads showed the widest range in *fer1l6* expression, which may be due in part to differences in follicular stages within the ovaries at the time of necropsy.

Loss of Fer1l6 leads to abnormal development

To determine the effects of a loss of Fer1l6 expression, we characterized a mutant line harboring a nonsense C to T transition on chromosome 9 at position 14112168 (GRCz10) that results in an early stop codon in exon 8 at amino acid position 237 (Supplemental Figure 1). To account for any genetic compensation that may occur in the mutant, we compared the mutant line to a splice blocking morpholino knockdown.

Both the mutant and the morpholino resulted in a slight developmental delay on 1 dpf, with obvious phenotypic differences observable on day 2 and beyond. Not all mutant larvae displayed a severe phenotype, suggesting incomplete penetrance. Among those displaying a phenotype, mortality began as early as 3 dpf, and reached 100% by day 5 (Supplemental Figure 2, B and C). In addition, relative to age-matched 1 dpf wild-type (WT) larvae, mutant larvae displayed reduced size and shortened trunk (Figure 2A). The abnormalities in head and trunk development were more pronounced at 2 dpf with both smaller, misshapen heads and smaller eyes (Figure 2B). In addition, the skeletal muscle of the trunk appeared disorganized and the myotomes did not exhibit the expected chevron shape (Figure 2B). Mutant larvae also displayed little to no blood circulation. By 3 dpf, morbidity increased significantly in mutant larvae with edema in the cranial, pericardial, and yolk sack areas. A severe spinal curvature and abnormal caudal fin morphology also appeared at 3 dpf.

Similar to mutant larvae, Fer1l6 morphant larvae displayed reduced head size and shortened trunk at 1 dpf (Figure 2C), with more pronounced head and trunk abnormalities at 2 dpf and increasing edema dorsal muscle deformities and spinal curvature as

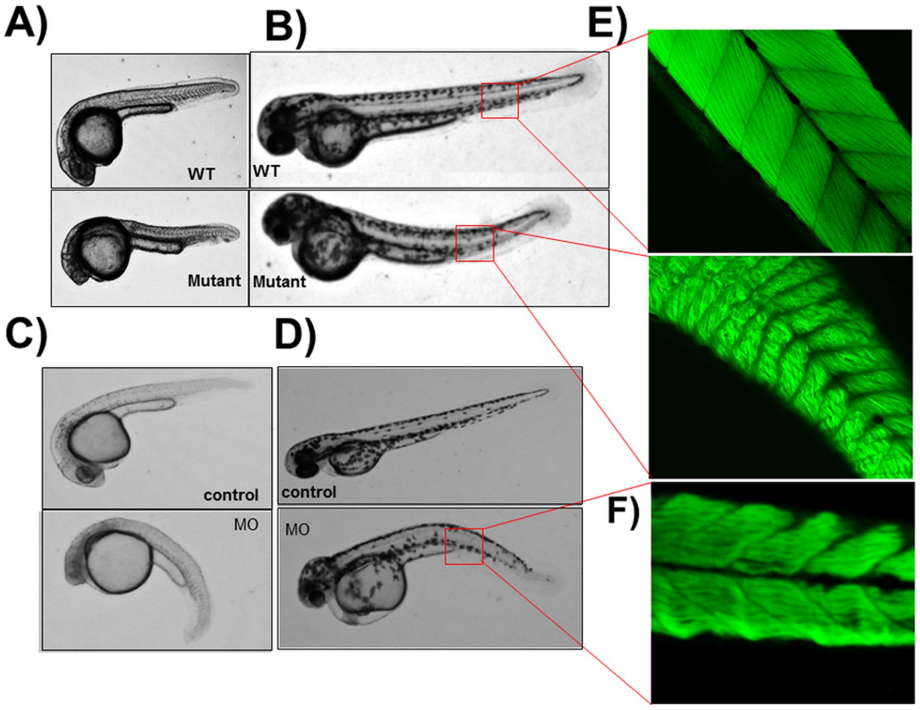

FIGURE 2: Loss of Fer1l6 results in muscle defects. Representative brightfield images of WT and fer1l6 mutant at (A) 1 dpf and (B) 2 dpf. Representative images of WT and morphant at (C) 1 dpf and (D) 2 dpf. (E) Phalloidin staining of WT (top panel) and fer1l6 mutant (bottom panel) skeletal muscle. (F) Phalloidin staining of morphant skeletal muscle.

development progressed (Figure 2D). Both Fer1l6-MO1 and Fer1l6-MO2 treatment produced similar phenotypes in a dose-dependent manner, with ~50% mortality by 5 dpf (Supplemental Figure 3). To eliminate the possibility that the morphant phenotype was due to off target effects owing to ectopic up-regulation of the p53 apoptosis pathway, the highest tested concentrations of Fer1l6-MO1 and Fer1l6-MO2 were coinjected with a p53 morpholino. These larvae exhibited the same phenotype as the Fer1l6-MO1 and Fer1l6-MO2 morphants, showing it is the result of a non-p53 pathway-dependent process (Supplemental Figure 3). For the remainder of our studies, 2.25 pmol Fer1l6-MO1 was used to achieve a maximal ~80% transcriptional knockdown with more than 95% of larvae exhibiting the phenotype.

Loss of Fer1l6 expression results in muscle defects

Fluorescein conjugated phalloidin was used to visualize myofibers in 2 dpf mutant and morphant larvae. Relative to WT and control larvae, both Fer1l6 mutant and morphant larvae displayed significant abnormalities in the patterning of actin filaments within the myotomes, with irregular myoseptum and bent myofibrils (Figure 2, E and F). To further characterize muscle development in the absence of Fer1l6, transmission electron microscopy (TEM) was employed on osmium stained longitudinal sections of 4 dpf larvae (Figure 3, A and B). Larvae depleted of Fer1l6 displayed a loss of striated muscle banding integrity and reduced t-tubule formation.

Both Fer1l6 mutant and morphants displayed pericardial edema, but after 2 dpf, mutants exhibited cranial, ocular, and yolk sac edema as well, while the morphant edema was principally pericardial and yolk sac (Supplemental Figure 3). To probe the effect of Fer1l6 depletion on cardiac development, we visualized control and Fer1l6-morphant larvae using a myosin heavy chain antibody at 4 dpf (Figure 3, C and D, and Supplemental Movies 1 and 2). This revealed that larvae with deficiencies in Fer1l6 expression exhibit myotube formation, but delayed chamber ballooning and valve formation relative to control. This phenotype was also associated with a statistically significant reduction in heart rate relative to control at 4 dpf (Figure 3E).

Abnormal muscle transcriptional profile in Fer1l6 mutant and morphant zebrafish

Given the observed muscle phenotype, we next sought to determine whether loss of Fer1l6 altered expression of muscle-related genes (Figure 4). We found that both mutant and morphant larvae exhibited greater than twofold inductions of dysferlin and myoferlin, suggestive of a compensatory activity. Given the function of myoferlin and dysferlin in myogenesis and muscle repair, we characterized the developmental state of both mutant and morphant larvae muscle by probing the expression of satellite cell (*pax7*), myogenic progenitor (*myod1*, *myf5*), and late-myocyte differentiating (*myog*, *myf4*) markers. Loss of Fer1l6 in the mutant (Figure 4, top) or with morpholino knockdown (Figure 4, bottom) resulted in a significant down-regulation of *pax7*, while differentiation markers *myod1*, *myf4*, and *myog* were significantly up-regulated. We also found *murf1*, a striated muscle-specific E3 ubiquitin ligase, to be up-regulated in both mutant and morphant while *atrogin-1*, another E3 ubiquitin ligase, was down-regulated in both Fer1l6 mutant and morphant models.

Characterization of Fer1l6 in mammalian cells

To establish a mammalian cell line by which to characterize Fer1l6, we probed for the protein in C2C12 cells, which are derived from mouse leg skeletal muscle (Yaffe and Saxel, 1977). Myoblast-to-myotube transition in C2C12 cells is initiated by reduction of serum in culture media, and samples were taken at days 0, 2, 6, and 10 under low serum conditions. To ensure that serum starvation for 10 d was sufficient for differentiation, we quantitated the number of nuclei-per-cell, and compared actinin and calsequestrin immunofluorescently labeled cells at 0- and 10-d differentiation. We found that relative to cells at D0, serum starved cells were multinucleated, and displayed actinin and calsequestrin labeling patterns consistent with previous reports of differentiated C2C12 cells (Supplemental Figure 4). Expression of *Fer1l6* mRNA was measured and compared with expression of dysferlin, which is known to change during the myoblast-to-myotube transition (Figure 5A; Belanto *et al.*, 2010). There was no significant difference in *Fer1l6* expression at any time point tested. By contrast, we found a significant increase in dysferlin mRNA levels under low serum conditions, consistent with previous studies (Belanto *et al.*, 2010). Analysis of results of Western blot probed for Fer1l6 and dysferlin at 0 and 10 d under low serum conditions confirmed the qPCR data (Figure 5B). Fer1l6 protein was present at a similar concentration at both time points, while dysferlin was detected at day 10 only (Figure 5B). Analysis of immunofluorescence imaging of Fer1l6 protein in undifferentiated C2C12 cells revealed the protein at the perinuclear region in puncta, as well as at the cell periphery (Figure 5C).

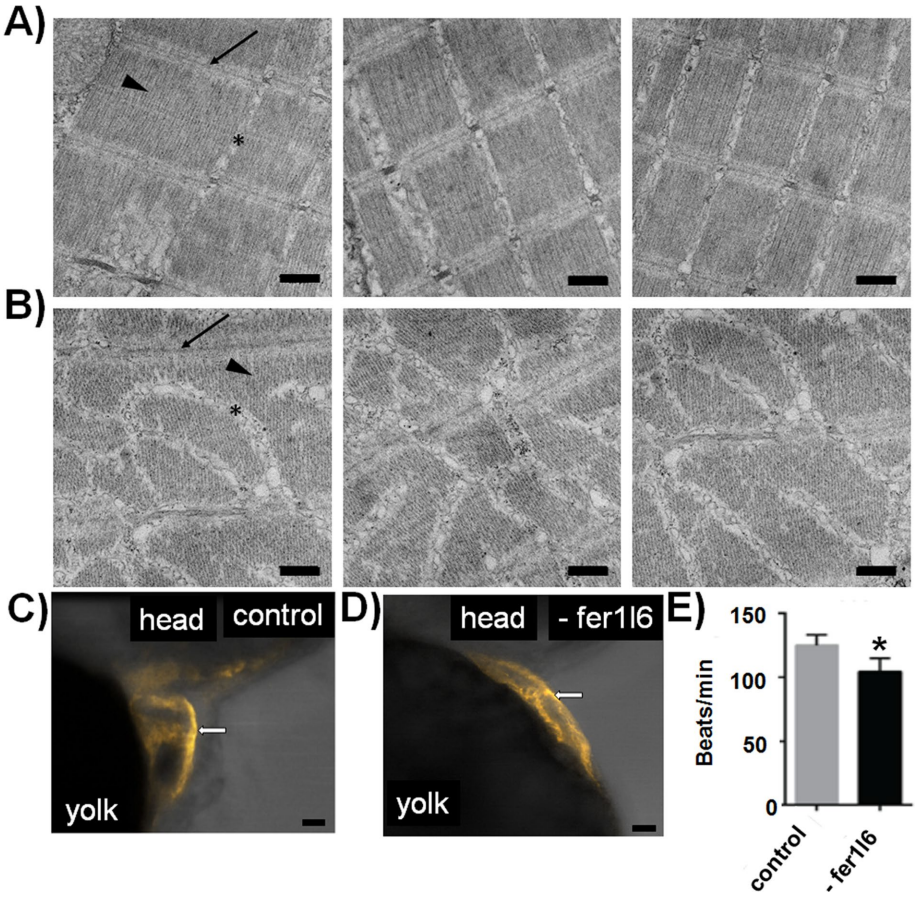

FIGURE 3: Loss of Fer1l6 results in skeletal muscle malformation and delayed heart development. Transmission electron microscopy images of (A) control and (B) morphant skeletal muscle sections. A band (denoted with arrowhead) and I band (denoted with arrow) patterning is severely disrupted by accumulation of disordered sarcoplasmic reticulum (denoted by an asterisk). Scale bar is 0.5 μm. (C) Immunostaining of sarcomere myosin in 4 dpf heart from control sample. Scale bar is 50 μm. (D) Immunostaining of sarcomere myosin in 4 dpf heart from morphant. Delayed development of distinct atrium and ventricle compartmentalization is evident. Arrows indicate heart valve. (E) Heart rate of control and morphant larvae at 4 dpf. *, $p < 0.05$, $n = 23$. Error bars represent SD.

Fer1l6 associates with lipid membranes, syntaxin 4 and vinculin

To characterize putative binding partners of Fer1l6, we immunoprecipitated Fer1l6 from C2C12 cell lysate and probed the samples by Western blot. We found that syntaxin 4 and vinculin coimmunoprecipitated with Fer1l6 (Figure 5D). By contrast, vimentin was not detected in Fer1l6 immunoprecipitated samples. To determine whether Fer1l6 and syntaxin 4 colocalize within C2C12 cells, we conducted proximity ligation assays (PLA; Mats *et al.*, 2011). To control for nonspecific Fer1l6 antibody absorption, we employed an anti-H3 histone antibody as a negative control. PLA analysis indicated that Fer1l6 colocalizes with both syntaxin 4 and vinculin, with a mean of nine and six puncta/cell, respectively, while no puncta were observed with FerL6 and anti-H3 (Figure 5, E and F). Both the syntaxin 4 and vinculin puncta were observed in both perinuclear and peripheral regions of the cell (Figure 5, E and F).

Finally, to test the membrane binding properties of the putative C2 domains of Fer1l6, we utilized an in vitro fluorescence-based assay. In this assay, positive shifts of the general polarization (GP) value of the liposome embedded probe laurdan provide a quantitative measure for protein–membrane interaction (Harris *et al.*, 2002; Marty *et al.*, 2013). We found the individual recombinant C2 domains (C2B, C2C, C2D, C2E, and C2F) bound to 1:4 POPS/POPC liposomes, while the maltose binding protein, which served as a negative control, did not interact with liposomes (Supplemental Figure 5; Marty *et al.*, 2013). The addition of 250 μM free Ca^{2+} enhanced C2-membrane interaction, consistent with previous reports of a Ca^{2+} enhanced protein–membrane interaction reported for otoferlin and dysferlin (Johnson and Chapman, 2010; Marty *et al.*, 2013; Abdullah *et al.*, 2014).

DISCUSSION

The ferlin gene family is thought to share an evolutionarily conserved function in calcium sensitive membrane trafficking (Lek *et al.*, 2010, 2012; Johnson, 2017). In this study we have discovered a role for Fer1l6. Not found in invertebrate genomes, Fer1l6 is thought to have emerged from a gene duplication event early in vertebrate evolution, and analysis of the phylogenetic tree in Figure 1 indicates that Fer1l6 is closer to otoferlin than to dysferlin or myoferlin. However, Fer1l6 is more broadly expressed than otoferlin, and appears to be necessary for proper myotome structure and myofibril formation. Further, the pronounced spinal curvature of the trunk and caudal tail deformities in both mutant and morphant larvae resemble abnormalities typically observed in congenital myopathies (Kawahara *et al.*, 2011). This phenotype differs from loss-of-function mutations in the Fer1l6 homologue otoferlin, which is expressed in sensory hair cells and regulates calcium-dependent neurotransmitter release (Roux *et al.*, 2006; Beurg *et al.*, 2008; Pangršič *et al.*, 2012; Chatterjee *et al.*, 2015). Like Fer1l6, the ferlin homologues dysferlin and myoferlin are expressed in muscle tissue; however, the phenotypes associated with knockout of either differ from our results (Davis *et al.*, 2000; Bansal *et al.*, 2003; Doherty *et al.*, 2005). For example, our observation of heart development deficiencies in Fer1l6 mutant zebrafish differs from reports of dysferlin or myoferlin knockout models, which are not believed to display heart development defects. However, a recent study on a myoferlin–dysferlin double knockout mouse model reported abnormal t-tubule formation and dilated sarcoplasmic reticulum that appears to partially phenocopy the Fer1l6 mutant (Demonbreun *et al.*, 2014). Examination of both Fer1l6 mutant and morphants revealed upregulation of myoferlin and dysferlin, suggesting that there may be some functional redundancy. The expression profile of Fer1l6 during myoblast-to-myotube transition is different from that of dysferlin, however, with Fer1l6 found in both C2C12 myoblasts and myotubes, while dysferlin expression is almost exclusively in myotubes. We conclude that Fer1l6 has diverged in timing, tissue specificity, and at least to some extent function, from other ferlins.

Fer1l6 appears to inhabit both perinuclear and cell membrane compartments, colocalizes with syntaxin 4, and binds membranes in a calcium enhanced manner. These findings are similar to previous

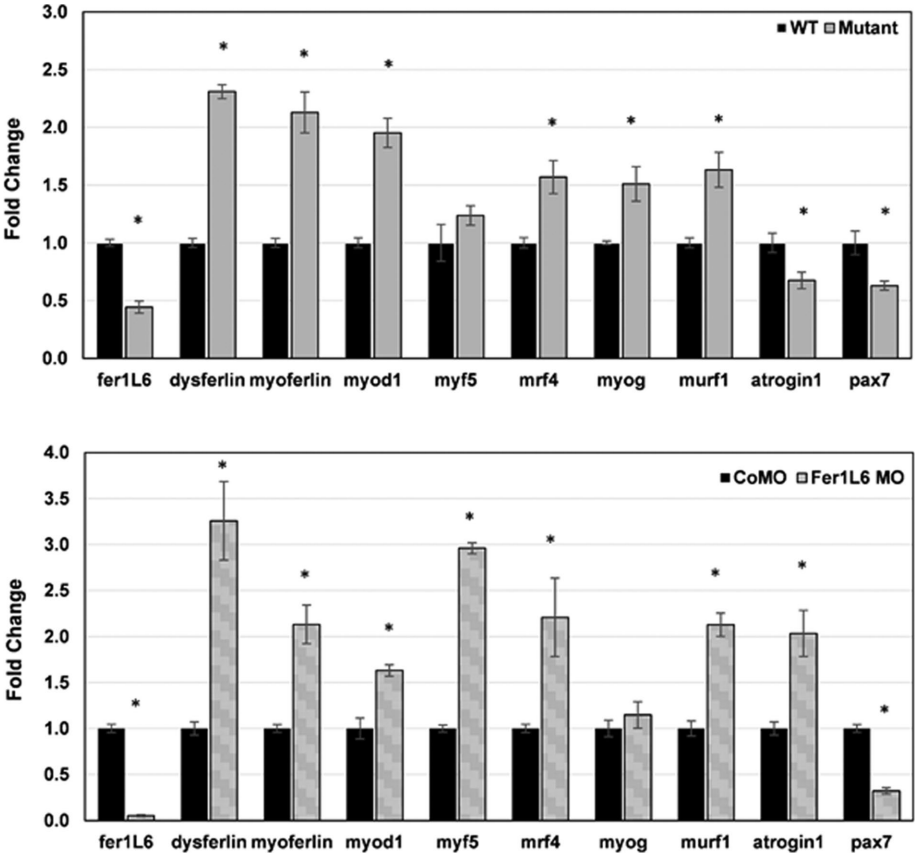

FIGURE 4: Transcriptional expression of muscle-specific genes in 2 dpf zebrafish. Loss of Fer1l6 in the mutant (top) or with morpholino knockdown (bottom) resulted in changes in transcripts associated with muscle development and maturation. Bars represent mean fold changes using ddCT method of qPCR analysis, plus or minus SEM. *, $p < 0.05$, $n = 3$ for wild type and mutant, $n = 4$ for control and morphant.

reports for dysferlin and otoferlin, and upholds the current hypothesis that ferlins function as calcium sensors for membrane trafficking events (Ramakrishnan *et al.*, 2009, 2014; Johnson and Chapman, 2010; Codding *et al.*, 2016). The C2 domains at the carboxy terminus of otoferlin are essential for exocytosis, and in general, the amino acid sequence is highly conserved among the ferlins, including Fer1l6 (Lek *et al.*, 2010; Pangršič *et al.*, 2010). Thus, although the physiological role of Fer1l6 appears distinct from other ferlins, we speculate that it retains similar functional properties with ferlin homologues at the carboxy terminus.

In addition to larvae, Fer1l6 expression was also found in adults, and was similar to the expression profile produced from RT-PCR of human cell line derived cDNA, where expression was observed in the lung and heart, with little expression in the brain (Redpath *et al.*, 2016). We also detected Fer1l6 in the gills and gonads of adult zebrafish, with peak fer1l6 expression occurring at 72 hpf, a developmental time associated with the onset of gill development (Kimmel *et al.*, 1995). Teleost gills contain neural crest-derived pillar cells, which play an important role in changing the functional respiratory surface area of gill lamellae by contracting or relaxing the smooth-muscle myosin within the cell (Nilsson, 2007; Mongera *et al.*, 2013). Like the gills, ovary maturation and follicular rupture/ovulation also involves contractile tissue and smooth-muscle myosins (Villeneuve *et al.*, 2010). We therefore speculate that Fer1l6 may play a similar role in these tissues as with heart and skeletal muscle.

Finally, our study reaffirms the use of zebrafish as a profitable model for the study of both the ferlin gene family and for identifying genetic factors that influence muscle physiology. Zebrafish models for both otoferlin and dysferlin have been previously reported, and the establishment of this Fer1l6 mutant strain adds a new resource from which to formulate comparisons between ferlin members (Kawahara *et al.*, 2011; Roostalu and Strähle, 2012; Chatterjee *et al.*, 2015).

MATERIALS AND METHODS

Zebrafish husbandry

Zebrafish (*Danio rerio*) were housed at the Sinnhuber Aquatic Research Laboratory (SARL) at Oregon State University (Corvallis, OR), according to Institutional Animal Care and Use Committee protocols. Adult WT 5D zebrafish were maintained on a recirculating system with water temperature of 28 ± 1°C on a 14:10 light/dark cycle. Spawning and embryo collection for gene expression studies and microinjections were conducted as previously described (Chatterjee *et al.*, 2015).

fer1l6sa16199 mutant line

Zebrafish carrying a point mutation in fer1l6 (fer1l6sa16199 strain) were originally identified through a targeting induced local lesions in genomes (TILLING) project in *N*-ethyl-*N*-nitrosourea (ENU)–mutagenized zebrafish as previously described (Wienholds *et al.*, 2003; Kurowska *et al.*, 2011). The mutants harbored a nonsense C to T transition on chromosome 9 at position 14112168 (GRCz10; Supplemental Figure 1). Heterozygous fer1l6sa16199, produced via in vitro fertilization of WT AB eggs with fer1l6sa16199 cryopreserved sperm, were purchased from the Zebrafish International Resource Center (Eugene, OR) and raised to adulthood at SARL on a flow-through system with water temperature of 28 ± 1°C on a 14:10 light/dark cycle. Offspring of heterozygous carriers were genotyped for the fer1l6sa16199 point mutation with genomic DNA isolated from caudal fin clips. Approximately 4-mo-old zebrafish were anesthetized with buffered tricaine methanesulfonate following institutionally approved protocols, fins were cut and placed in individual wells of a 96-well qPCR plate, and the fish were allowed to recover in individual tanks until the genotyping procedure was completed. Fins were lysed with 50 mM NaOH at 95°C for 20 min or until dissolved and then neutralized 1:10 with 1 M Tris and diluted threefold with ultrapure H_2O. PCR amplification of genomic DNA with custom-made TaqMan single-nucleotide polymorphism probes for the two different alleles, designed based on manufacturers recommendation (Thermo Fisher Scientific), was performed with a StepOnePlus Real-Time PCR System (Applied Biosystems). PCR products were sent for sequencing to confirm the genotype of fer1l6+/+ and fer1l6sa16199, hereafter WT and mutant, respectively. The mutant and WT lines were maintained through subsequent spawning. Developmental observations were made following multiple spawning events from a random grouping of male and female fer1l6sa16199, and compared with development of WT counterparts from WT spawning events. Embryos were collected following

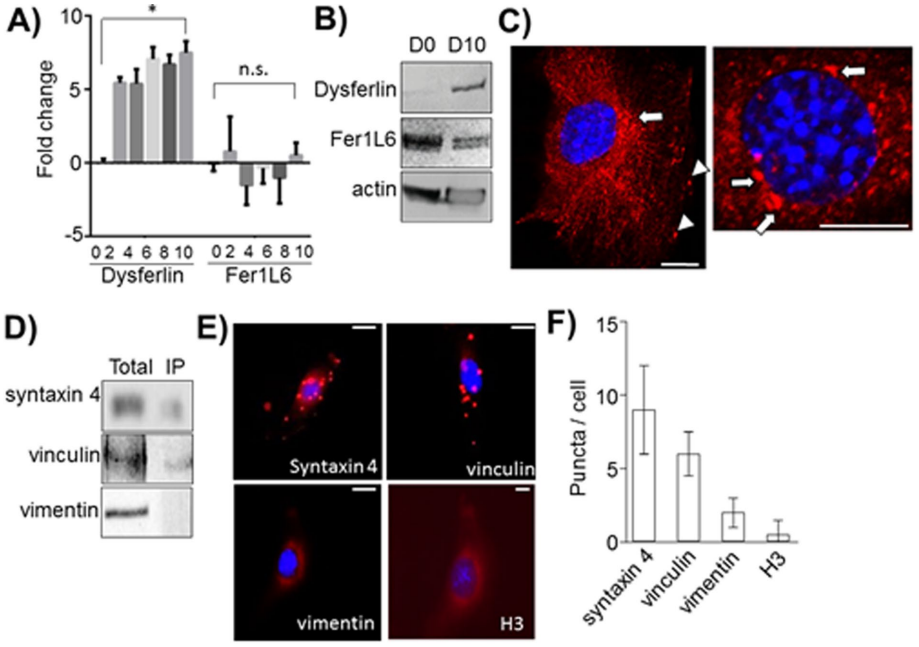

FIGURE 5: Characterization of Fer1l6 in C2C12 cell culture. (A) Dysferlin and Fer1l6 expression at days 0, 2, 4, 6, 8, and 10 after serum starvation. *, $p < 0.05$, n.s. = not significant, $n = 3$. (B) Western blot of C2C12 cell lysate at days 0 and 10 under serum starvation conditions probed for dysferlin, Fer1l6, and actin. (C) Representative images of Fer1l6 (red) and Hoechst (blue) stained C2C12 cells. Fer1l6 forms puncta at the perinuclear region (arrows) and at the cell periphery (arrowheads). The magnified image on the right illustrated the Fer1l6 patches in the perinuclear region. Scale bar is 10 μm. (D) Immunoblot of C2C12 lysate immunoprecipitated (IP) with an anti-Fer1l6 antibody and probed with anti–syntaxin 4, anti-vinculin, and anti-vimentin antibodies. Total corresponds to lysate before immunoprecipitation. Images are representative of three separate samples. (E) Representative images of individual C2C12 cells after proximity ligation labeling for syntaxin 4, vinculin, vimentin, and H3. Red puncta indicate colocalized protein; the nucleus was stained with Hoechst. Scale bar is 10 μm. (F) Quantitation of proximity ligation results. Error bars represent SD, $n = 4$.

spawning, and placed in individual wells of 96-well plates with 100 μl of embryo media. Embryos were observed in the morning daily, and the presence of any developmental abnormality was recorded along with mortality. The occurrence of a Fer1l6 loss-of-function phenotype occurred in ~15% of spawned larvae.

Microinjections

Morpholinos (MOs) to target intron–exon boundaries were designed for zebrafish fer1l6 following manufacturer recommendations (GeneTools). Fer1l6-MO1 targeted intron 14 to exon 15 with a sequence of CTCCCTCTTCctgacaaacataaaa, and Fer1l6-MO2 targeted intron 2 to exon 3 with a sequence of AGCCTCTATCGTGTaacgattaaac, where lowercase letters represent the intron-specific sequence and uppercase letters represent the exon-specific sequence (Supplemental Figure 1). Both MOs would presumably result in the loss of their respective exon, and ultimately an early stop codon due to a frameshift. In addition to custom-designed MO targets, a MO standard control oligo and a p53 targeting MO were also used for the Fer1l6 knockdown studies. All microinjections were performed with WT 5D zebrafish as previously described (Chatterjee *et al.*, 2015). Embryos were observed in the morning daily, and the presence of any developmental abnormality was recorded along with mortality. Heart rate was measured manually at 96 h postfertilization by counting the pulse of blood through the chambers of the heart for 20 s and multiplying by 3. The experiment was repeated twice, with an $N = 20–23$ for control and for Fer1l6-MO1 morphants in each replicate.

RNA isolation and qPCR analysis

Total RNA was isolated from whole larvae at a given time point or from adult tissue using RNAzol RT (Molecular Research Center, Cincinnati, OH). RNA was converted to cDNA using the Applied Biosystems High-Capacity cDNA Reverse Transcription kit (Life Technologies, Carlsbad, CA), and qRT–PCR for target genes was performed using Power SYBR Green PCR Master Mix with a 7500 Fast Real-Time (Applied Biosystems, Foster City, CA). Primers were purchased from Integrated DNA Technologies (Coralville, IA), including β-actin, which was used as a housekeeping gene for normalization. Relative gene expression was quantified using the ΔΔCt method (Pfaffl, 2001) for all genes during developmental time points. For adult tissues, samples were normalized to the average β-actin within sex and tissue type, and a standard curve was used to quantify fer1l6 transcript in a given tissue sample.

For C2C12 cells, an RNAeasy kit (Quiagen, Germany) was used to extract total RNA from cells according to manufactures' protocol. cDNA was synthesized using an iScript DNA synthesis kit (Bio-Rad) according to the manufacturer's protocol. All qPCR was performed using Power SYBR-Green PCR Master Mix (Applied Biosystems) on a 7500 fast Real-Time PCR System (Applied Biosystems). Primers for target genes were purchased from Sigma-Aldrich Custom design probes.

Whole–mount ISH

ISH was performed on WT 5D zebrafish embryos with digoxigenin (DIG)-labeled antisense RNA probes designed to hybridize to a unique region of the fer1l6 zebrafish mRNA (NCBI accession number NW_001879462.3), with a forward primer 5′-ATGGACCAABTAAAGCAGCTCTGCAC-3′ and the T7 reverse complement 5′-TAATACGACTCACTATAGGGCCACACTGGATCTGCTGAGCTC-3′. The design and detection of the probe with anti-DIG alkaline phosphatase conjugated antibody was performed as previously described (Chatterjee *et al.*, 2015).

Electron microscopy

Control MO and Fer1l6-MO1 injected zebrafish were fixed in 2.5% glutaraldehyde and osmium staining was performed sing 1% osmium tetroxide and 0.8% potassium ferricyanide. Resin imbedding was performed using EMbed-812 (Electron Microscopy Sciences) according to the manufacturer's protocol. Ultramicrotomy sectioning was performed at 50 nm using a diamond blade microtome, and placed on copper PELCO formvar-coated grids (TedPella). Imaging was performed on a FEI Titan 80-20 TEM microscope at Oregon State University.

Immunostaining and fluorescence microscopy

Zebrafish larvae were fixed in 4% paraformaldehyde (PFA) overnight at 4°C, and then washed three times in phosphate-buffered saline (PBS), pH 7.4, before fluorescence staining. For visualization

of muscle structure, phalloidin conjugated to the green fluorescent dye fluorescein was used (Thermo Fisher Scientific). Tissue was permeabilized using 2% Triton X-100 in PBS for 90 min, followed by three washes with PBS. Larvae were then incubated in 1:2000 fluorescein–phalloidin in PBS for 1 h at room temperature, followed by three washes in PBS and 0.1% Tween 20 (PBST). Larvae were mounted on coverslips and confocal imaging was performed as previously described (Almlie *et al.*, 2016). To visualize the heart structure, a monoclonal antibody that recognizes the heavy chain of myosin II (MF20; Thermo Fisher Scientific) was used with both control MO and Fer1l6-MO1 injected fish. Cardiac sarcomeres were visualized using confocal microscopy (Zeiss LSM 780 NLO).

C2C12 cells were cultured in DMEM with 10% fetal bovine serum (Thermo Fisher Scientific) on glass rat tail collagen coated coverslips. Coverslips were fixed in 4% PFA in PBS for 15 min and then washed in PBS. Cells were permeabilized in 0.1% Triton X-100 for 10 min and then washed in PBS. Cells were blocked in 5% normal goat serum and 1% bovine serum albumin in PBST for 1 h followed by the addition of primary Fer1l6 antibody (Abcam, UK) at 1:500, calsequestrin 2 (Proteintech) at 1:200, alpha sarcomeric actinin (Thermo Fisher Scientific) at 1:100, and myosin heavy chain (Developmental Studies Hybridoma Bank) at 1:200, and incubated overnight at 4°C. Cells were washed in PBS and then secondary antibody was added at 1:1000 + 4′6′-diamidino-2-phenylindole (DAPI) at 1:2000 and incubated for 1 h at room temperature. After washing, coverslips were mounted in ProLong Gold Antifade Mountant (Thermo Fisher Scientific) for imaging. Images were collected on a Zeiss LSM 780 NLO confocal microscope. Postimaging processing was performed using Zen black.

Western blot

Western blot was carried out as previously described (Johnson and Chapman, 2010). Samples were run on 8% gel, blotted onto polyvinylidene fluoride (PVDF) membrane, and blocked with 2% milk in PBST. Proteins were detected with primary antibodies at 1:500 and secondary antibodies at 1:1000. Hamlet anti-dysferlin, anti-Fer1l6, and anti-actin were purchased from Abcam (Cambridge, MA).

Proximity ligation assay

C2C12 cells were grown in sterile six-well plates (Sigma). After the cells reached 70% confluence, they were washed in PBS and then fixed with 4% PFA for 10 min at room temperature. Fixed cells were subsequently washed, permeabilized with 0.2% Triton X-100 for 10 min, and blocked with Duolink blocking buffer for 1 h at 37°C. Each sample was then incubated with primary antibodies in Duolink diluent at 4°C (goat anti-Fer1l6, 1:250; Santa Cruz Biotech; rabbit anti–syntaxin 4, 1:500; Sigma; rabbit anti-vinculin 1:500; Sigma; rabbit anti-histone H3 1:500; Sigma; rabbit anti-vimentin 1:500; Sigma). Samples were subsequently washed and incubated with Duolink proximity ligation probes for 1 h at 37°C. Cells were then washed and two oligonucleotides complementary to the individual proximity ligation assay probes were added in the presence of a ligation enzyme per the manufacturer's protocol, and incubated for 30 min at 37°C. The samples were subsequently subjected to rolling circular amplification for 100 min at 37°C in the presence of labeled complimentary oligonucleotide probes. Finally, samples were stained with Hoechst stain and mounted on glass slides with Fluoromount (Life Technologies).

Statistics

All data were analyzed using a *t* test with a significance value set at $p \leq 0.05$ using either GraphPad or SigmaPlot statistical software. For qPCR data within a single developmental time period, significant fold changes were relative control. For qPCR data over several time periods, significant fold changes were relative to the first time point collected. *t* tests were also used to determine sex-specific differences in fer1l6 expression in adult zebrafish organs, changes in heart rate between control and Fer1l6-MO1 morphants, and to determine the effect of calcium on the liposome binding assay.

Cloning Fer1l6 domains

Plasmid puc57-Fer1l6 was used as a template for amplification of each Fer1l6 domain. Forward and reverse primers were designed to amplify the 5′ and 3′ coding sequence of each domain: C2B (amino acids 77–174), C2C (amino acids 237–344), C2D (amino acids 818–926), C2E (amino acids 1007–1090), and C2F (amino acids 1349–1450). A LIC sequence was added to both ends of the forward and reverse primers, so the amplicons would adhere to a SSPI/T4-treated pMCSG9 vector. Both vector and amplicons were mixed and ligated with T4 DNA ligase. The plasmids were then transformed into *Escherichia coli* DH5α cells. The sequences in the colonies were checked by GenScript before being retransformed into *E. coli* BL21 cells.

Protein expression

For each his-tagged MBP Fer1l6 domain, the BL21 cells were grown in lysogeny broth (LB) for 18 h at 250 rpm at 37°C. They were then transferred to fresh LB and were incubated at 37°C until their optical density reached 0.6. The cells were induced with 1 mM isopropyl β-D-1-thiogalactopyranoside before being incubated for 4 h. The cells were centrifuged at 4000 rpm before using a microfluidizer to lyse the cells with lysis buffer (20 mM phosphate, 150 mM NaCl, 10 mM imidazole, pH 7.5). Pepstatin A (1 µg/ml), leupeptin (1 µg/ml), and phenylmethane sulfonyl fluoride (1 mM) were added. The cell lysate was centrifuged at 2000 rpm until insoluble cellular components formed a pellet. The soluble domains were then purified with high density nickel agarose beads and washed with 20 bed volumes of lysis buffer before elution with two bed volumes of elution buffer (20 mM phosphate, 150 mM NaCl, 500 mM imidazole, pH 7.4). The proteins were dialyzed for 16 h with 1× PBS (20 mM phosphate, 150 mM NaCl, pH 7.4) at 4°C.

Liposome binding

Liposomes were prepared as described previously (Marty *et al.*, 2013). Briefly, a chloroform solution containing a lipid mixture composed of a 1:1 ratio of POPS POPC with 2.5 mol% laurdan (Sigma) was dried under vacuum until the chloroform solvent was evaporated. The lipids were then rehydrated in buffer and extruded using a membrane with a 50-nm cutoff. Extruder, syringes, and membranes were purchased from Avanti Polar Lipids. A QM-40 instrument with Glan Thompson polarizers (Photon Technology International, Birmingham, NJ), was utilized for collection of the fluorescence measurements. All measurements were obtained at 37°C in 1× PBS (pH 7.5). The fluorophore laurdan was excited at wavelength 350 nm, and the GP value was measured based on the following equation: GP = (I430 – I480)/(I430 + I480), where I430 and I480 are the intensities emitted by laurdan at wavelengths 430 and 480 nm, respectively.

ACKNOWLEDGMENTS

This work was supported by funds provided by Oregon State University and by National Institutes of Health, National Institute of Deafness and Other Communication Disorders (NIDCD) Grant no. 1R01DC014588.

REFERENCES

Abdullah N, Padmanarayana M, Marty NJ, Johnson CP (2014). Quantitation of the calcium and membrane binding properties of the C2 domains of dysferlin. Biophys J 106, 382–389.

Almlie CK, Hsiao A, Burrows SM (2016). Dye-specific wavelength offsets to resolve spectrally overlapping and co-localized two-photon induced fluorescence. Anal Chem 88, 1462–1467.

Anderson LV, Davison K, Moss JA, Young C, Cullen MJ, Walsh J, Johnson MA, Bashir R, Britton S, Keers S, *et al*. (1999). Dysferlin is a plasma membrane protein and is expressed early in human development. Hum Mol Genet 8, 855–861.

Bansal D, Campbell KP (2004). Dysferlin and the plasma membrane repair in muscular dystrophy. Trends Cell Biol 14, 206–213.

Bansal D, Miyake K, Vogel SS, Groh S, Chen CC, Williamson R, McNeil PL, Campbell KP (2003). Defective membrane repair in dysferlin-deficient muscular dystrophy. Nature 423, 1–5.

Belanto JJ, Diaz-Perez SV, Magyar CE, Maxwell MM, Yilmaz Y, Topp K, Boso G, Jamieson CH, Cacalano NA, Jamieson CAM (2010). Dexamethasone induces dysferlin in myoblasts and enhances their myogenic differentiation. Neuromuscul Disord 20, 111–121.

Beurg M, Safieddine S, Roux I, Bouleau Y, Petit C, Dulon D (2008). Calcium- and otoferlin-dependent exocytosis by immature outer hair cells. J Neurosci 28, 1798–1803.

Cacciottolo M, Numitone G, Aurino S, Caserta IR, Fanin M, Politano L, Minetti C, Ricci E, Piluso G, Angelini C, *et al*. (2011). Muscular dystrophy with marked dysferlin deficiency is consistently caused by primary dysferlin gene mutations. Eur J Hum Genet 19, 974–980.

Chatterjee P, Padmanarayana M, Abdullah N, Holman CL, LaDu J, Tanguay RL, Johnson CP (2015). Otoferlin deficiency in zebrafish results in defects in balance and hearing: rescue of the balance and hearing phenotype with full-length and truncated forms of mouse otoferlin. Mol Cell Biol 35, 1043–1054.

Codding SJ, Marty N, Abdullah N, Johnson CP (2016). Dysferlin binds SNAREs (soluble *N*-ethylmaleimide-sensitive factor (NSF) attachment protein receptors) and stimulates membrane fusion in a calcium-sensitive manner. J Biol Chem 291, 14575–14584.

Davis DB, Delmonte AJ, Ly CT, McNally EM (2000). Myoferlin, a candidate gene and potential modifier of muscular dystrophy. Hum Mol Genet 9, 217–226.

Demonbreun AR, Rossi AE, Alvarez MG, Swanson KE, Deveaux HK, Earley JU, Hadhazy M, Vohra R, Walter GA, Pytel P, *et al*. (2014). Dysferlin and myoferlin regulate transverse tubule formation and glycerol sensitivity. Am J Pathol 184, 248–259.

Doherty KR, Cave A, Davis DB, Delmonte AJ, Posey A, Earley JU, Hadhazy M, McNally EM (2005). Normal myoblast fusion requires myoferlin. Development 132, 5565–5575.

Hams N, Padmanarayana M, Qiu W, Johnson CP (2017). Otoferlin is a multivalent calcium-sensitive scaffold linking SNAREs and calcium channels. Proc Natl Acad Sci USA 114, 8023–8028.

Harris FM, Best KB, Bell JD (2002). Use of Laurdan fluorescence intensity and polarization to distinguish between changes in membrane fluidity and phospholipid order. Biochim Biophys Acta 1565, 123–128.

Johnson CP (2017). Emerging functional differences between the synaptotagmin and ferlin calcium sensor families. Biochemistry 56, 6413–6417.

Johnson CP, Chapman ER (2010). Otoferlin is a calcium sensor that directly regulates SNARE-mediated membrane fusion. J Cell Biol 191, 187–197.

Kawahara G, Serafini PR, Myers JA, Alexander MS, Kunkel LM (2011). Characterization of zebrafish dysferlin by morpholino knockdown. Biochem Biophys Res Commun 413, 358–363.

Kerr JP, Ziman AP, Mueller AL, Muriel JM, Kleinhans-Welte E, Gumerson JD, Vogel SS, Ward CW, Roche JA, Bloch RJ (2013). Dysferlin stabilizes stress-induced Ca2+ signaling in the transverse tubule membrane. Proc Natl Acad Sci USA 110, 20831–20836.

Kimmel CB, Ballard WW, Kimmel SR, Ullmann B, Schilling TF (1995). Stages of embryonic development of the zebrafish. Dev Dyn 203, 253–310.

Kurowska M, Daszkowska-Golec A, Gruszka D, Marzec M, Szurman M, Szarejko I, Maluszynski M (2011). TILLING: a shortcut in functional genomics. J Appl Genet 42, 371–390.

Lek A, Evesson FJ, Sutton RB, North KN, Cooper ST (2012). Ferlins: regulators of vesicle fusion for auditory neurotransmission, receptor trafficking and membrane repair. Traffic 13, 185–194.

Lek A, Lek M, North KN, Cooper ST (2010). Phylogenetic analysis of ferlin genes reveals ancient eukaryotic origins. BMC Evol Biol 10, 231.

Liu Z, Shao Y, Tan L, Shi H, Chen S, Guo J (2014). Clinical significance of the low expression of FER1L4 in gastric cancer patients. Tumour Biol 3, 9613–9617.

Marlin S, Feldmann D, Nguyen Y, Rouillon I, Loundon N, Jonard L, Bonnet C, Couderc R, Garabedian EN, Petit C, *et al*. (2010). Temperature-sensitive auditory neuropathy associated with an otoferlin mutation: deafening fever! Biochem Biophys Res Commun 394, 737–742.

Marty NJ, Holman CL, Abdullah N, Johnson CP (2013). The C2 domains of otoferlin, dysferlin, and myoferlin alter the packing of lipid bilayers. Biochemistry 52, 5585–5592.

Mats G, Charlotta G, Simon F (2011). Duolink-"in-cell Co-IP" for visualization of protein interactions *in situ*. Nat Methods 8, 982.

Mongera A, Singh AP, Levesque MP, Chen Y-Y, Konstantinidis P, Nusslein-Volhard C (2013). Genetic lineage labeling in zebrafish uncovers novel neural crest contributions to the head, including gill pillar cells. Development 140, 916–925.

Nilsson GE (2007). Gill remodeling in fish—a new fashion or an ancient secret? J Exp Biol 210, 2403–2409.

Pangršič T, Lasarow L, Reuter K, Takago H, Schwander M, Riedel D, Frank T, Tarantino LM, Bailey JS, Strenzke N, *et al*. (2010). Hearing requires otoferlin-dependent efficient replenishment of synaptic vesicles in hair cells. Nat Neurosci 13, 869–876.

Pangršič T, Reisinger E, Moser T (2012). Otoferlin: a multi-C_2 domain protein essential for hearing. Trends Neurosci 35, 671–680.

Pfaffl MW (2001). A new mathematical model for relative quantification in real-time RT-PCR. Nucleic Acids Res 29, e45.

Posey AD, Pytel P, Gardikiotes K, Demonbreun AR, Rainey M, George M, Band H, McNally EM (2011). Endocytic recycling proteins EHD1 and EHD2 interact with Fer-1-like-5 (Fer1L5) and mediate myoblast fusion. J Biol Chem 286, 7379–7388.

Posey AD, Swanson KE, Alvarez MG, Krishnan S, Earley JU, Band H, Pytel P, McNally EM, Demonbreun AR (2014). EHD1 mediates vesicle trafficking required for normal muscle growth and transverse tubule development. Dev Biol 387, 179–190.

Ramakrishnan NA, Drescher MJ, Drescher DG (2009). Direct interaction of otoferlin with syntaxin 1A, SNAP-25, and the L-type voltage-gated calcium channel $Ca_v1.3$. J Biol Chem 284, 1364–1372.

Ramakrishnan NA, Drescher MJ, Morley BJ, Kelley PM, Drescher DG (2014). Calcium regulates molecular interactions of otoferlin with SNARE proteins required for hair cell exocytosis. J Biol Chem 289, 8750–8766.

Redpath GMI, Sophocleous RA, Turnbull L, Whitchurch CB, Cooper ST (2016). Ferlins show tissue-specific expression and segregate as plasma membrane/late endosomal or trans-Golgi/recycling ferlins. Traffic 17, 245–266.

Rodríguez-Ballesteros M, Reynoso R, Olarte M, Villamar M, Morera C, Santarelli R, Arslan E, Medá C, Curet C, Völter C, *et al*. (2008). A multicenter study on the prevalence and spectrum of mutations in the otoferlin gene (OTOF) in subjects with nonsyndromic hearing impairment and auditory neuropathy. Hum Mutat 29, 823–831.

Roostalu U, Strähle U (2012). In vivo imaging of molecular interactions at damaged sarcolemma. Dev Cell 22, 515–529.

Roux I, Safieddine S, Nouvian R, Grati M, Simmler MC, Bahloul A, Perfettini I, Le Gall M, Rostaing P, Hamard G, *et al*. (2006). Otoferlin, defective in a human deafness form, is essential for exocytosis at the auditory ribbon synapse. Cell 127, 277–289.

Smith MK, Wakimoto BT (2007). Complex regulation and multiple developmental functions of misfire, the *Drosophilamelanogaster* ferlin gene. BMC Dev Biol 7, 21.

Turtoi A, Blomme A, Bellahcène A, Gilles C, Hennequière V, Peixoto P, Bianchi E, Noel A, De Pauw E, Lifrange E, *et al*. (2013). Myoferlin is a key regulator of EGFR activity in breast cancer. Cancer Res 73, 5438–5448.

Villeneuve DL, Garcia-Reyero N, Martinović D, Cavallin JE, Mueller ND, Wehmas LC, Kahl MD, Linnum AL, Perkins EJ, Ankley GT (2010). Influence of ovarian stage on transcript profiles in fathead minnow (*Pimephalespromelas*) ovary tissue. Aquat Toxicol 98, 354–366.

Wang WS, Liu XH, Liu LX, Lou WH, Jin DY, Yang PY, Wang XL (2013). ITRAQ-based quantitative proteomics reveals myoferlin as a novel prognostic predictor in pancreatic adenocarcinoma. J Proteomics 91, 453–465.

Washington NL, Ward S (2006). FER-1 regulates Ca^{2+}-mediated membrane fusion during *C. Elegans* spermatogenesis. J Cell Sci 119 (Pt 12), 2552–2562.

Wienholds E, van Eeden F, Kosters M, Mudde J, Plasterk RHA, Cuppen E (2003). Efficient target-selected mutagenesis in zebrafish. Genome Res 13, 2700–2707.

Xia T, Chen S, Jiang Z, Shao Y, Jiang X, Li P, Xiao B, Guo J (2015). Long noncoding RNA FER1L4 suppresses cancer cell growth by acting as a competing endogenous RNA and regulating PTEN expression. Sci Rep 5, 13445.
Yaffe D, Saxel O (1977). Serial passaging and differentiation of myogenic cells isolated from dystrophic mouse muscle. Nature 270, 725–727.
Yasunaga S, Grati M, Cohen-Salmon M, El-Amraoui A, Mustapha M, Salem N, El-Zir E, Loiselet J, Petit C (1999). A mutation in OTOF, encoding otoferlin, a FER-1-like protein, causes DFNB9, a nonsyndromic form of deafness. Nat Genet 21, 363–369.
Yu C, Sharma A, Trane A, Utokaparch S, Leung C, Bernatchez P (2011). Myoferlin gene silencing decreases Tie-2 expression in vitro and angiogenesis in vivo. Vascul Pharmacol 55, 26–33.